

SCIENTIFIC REPORTS

OPEN

Multishock Compression Properties of Warm Dense Argon

Jun Zheng¹, Qifeng Chen¹, Gu Yunjun¹, Zhiguo Li¹ & Zhijun Shen²

Received: 25 June 2015

Accepted: 05 October 2015

Published: 30 October 2015

Warm dense argon was generated by a shock reverberation technique. The diagnostics of warm dense argon were performed by a multichannel optical pyrometer and a velocity interferometer system. The equations of state in the pressure-density range of 20–150 GPa and 1.9–5.3 g/cm³ from the first- to fourth-shock compression were presented. The single-shock temperatures in the range of 17.2–23.4 kK were obtained from the spectral radiance. Experimental results indicates that multiple shock-compression ratio ($\eta_i = \rho_i/\rho_0$) is greatly enhanced from 3.3 to 8.8, where ρ_0 is the initial density of argon and ρ_i ($i = 1, 2, 3, 4$) is the compressed density from first to fourth shock, respectively. For the relative compression ratio ($\eta'_i = \rho_i/\rho_{i-1}$), an interesting finding is that a turning point occurs at the second shocked states under the conditions of different experiments, and η'_i increases with pressure in lower density regime and reversely decreases with pressure in higher density regime. The evolution of the compression ratio is controlled by the excitation of internal degrees of freedom, which increase the compression, and by the interaction effects between particles that reduce it. A temperature-density plot shows that current multishock compression states of argon have distributed into warm dense regime.

The physical properties of warm dense matter (WDM) are a challenging field of research¹. Generally, WDM covers the states of matter with the density-temperature range of 10^{22} – 10^{25} cm⁻³ and 0.1–100 eV. In this regime, matter is strongly coupled ($1 < \Gamma < 100$), mostly degenerate ($\Theta = k_B T/E_F \sim 1$), and non-ideal². Recently, WDM in the partial ionization regime is also becoming one of important research topics^{3–7}. The existence of much challenge boosts the development of experiments and theories as the equations of state (EOSs) and the compression technique.

Argon is usually considered as a model substance in WDM region, whose experimental data of EOSs can be used to test and verify the theoretical models. For the purpose, existing experiments reveal that the principal Hugoniot measurements of solid⁸ and liquid^{9,10} argon have been performed, and liquid argon has been single-shocked up to the pressure of 91 GPa. The single-shock data were reproduced by a fluid variational theory¹¹, which did not include the ionization effect. For the multiple shock compression technique, the obtained data can efficiently extend the applicable range of the models in WDM regime, but it has not been used for argon.

Double-shock data were deduced by the interface continuity condition and strongly depend on the EOSs of the rear anvil, which have been applied in helium¹², deuterium¹³, and xenon¹⁴. Several theoretical simulations including QMD¹⁵, PIMC^{15,16}, and the chemical pictures^{13,17}, have been performed, but none of them could give a creditable prediction of the WDM states for different materials. For dense gaseous mixtures of H₂+He¹⁸, and H₂+D₂¹⁹, limited third-shock compression data were obtained by the spectral radiance histories of the specimen on the premise of good shock transparency of the anvil interface. Though the shock reverberation technique has been applied to the EOSs study^{20,21,22}, the determination of multiply compressed states were done with the help of hydrodynamic simulations. By now, the integrated multishock compression states diagnostics have not been reported, and shock data of argon above the

¹Laboratory of Shock Wave and Detonation Physics, Institute of Fluid Physics, P.O. Box 919-102, Mianyang, Sichuan, P. R. China. ²Laboratory of computational Physics, Institute of Applied Physics and Computational Mathematics, P. O. Box 8009-26, Beijing, P. R. China. Correspondence and requests for materials should be addressed to Q.C. (email: chenqf01@gmail.com)

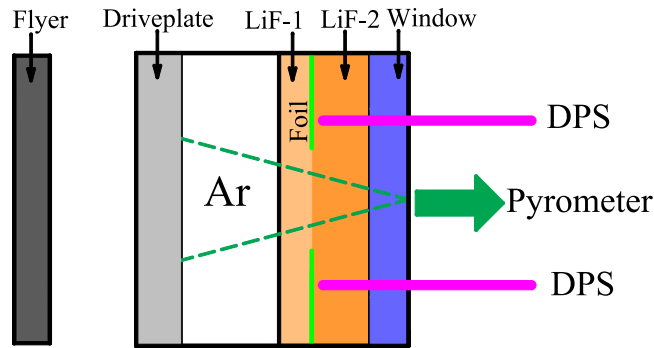


Figure 1. Schematic view of the experimental target and diagnostic devices used to obtain the EOSs of warm dense argon.

100 GPa range are scarce. In addition, no experiment for argon involves in the temperature measurement, which should give an important test for theoretical models.

In our previous work, multiple compression argon⁴ with lower initial densities has been reported. However, it was not integrated especially for the third-shock state and the shock temperature. In this paper, the integrated state diagnostics of argon from single- to fourth-shock compression are developed with an optical pyrometer and a velocity interferometer system. Multishock pressure-density up to 150 GPa and 5.3 g/cm^3 are obtained. The single-shock temperatures of 17.2–23.4 kK are obtained from the spectral radiance before the loss of the interface transparency appears. Based on these results, we will discuss the evolution of multishock compression properties, and the coupling and the degeneracy parameters of the multishock compression states in the temperature-density plane.

Results

The multishock reverberation technique is widely applied to produce WDM. In our experiments, Fig. 1 shows the experimental target and diagnostic devices used to obtain the EOSs of warm dense argon. Before the experiment, the argon specimen was precompressed to about 40 MPa at the surrounding temperature, and the initial density was measured by a method of draining with a special pressure vessel²³. In the experiment, the representative multishock spectral radiance histories were measured by a pyrometer and the particle velocity profile histories were measured by a Doppler pins system (DPS)²⁴, which are shown in Fig. 2(a) for the shot of No. GAr-4. The self-emission spectral radiance provides a clear indication of shock arrival at the corresponding interface of the experimental target cell in Fig. 2(a). Multishock compression states can be determined as follows.

(I) The nearly flat regime (between time t_0 and t_1) indicates that the shock wave propagates steadily through the argon specimen, where warm dense argon with good uniformity is generated. The 1st shock velocity (U_{s1}) was obtained according to the crossing time and the thickness of the specimen chamber (including the distortion in the precompressed state). The 1st shock particle velocity, pressure, and density (U_{p1} , P_1 , and ρ_1) of argon were determined using an impedance matching method to solve the Rankine-Hugoniot equations²⁵. The single-shock temperature (T_1) was obtained from the spectral radiance.

(II) When the shock reached the specimen/LiF-1 interface, the transparency was partially lost due to high shock temperature. As a result, a lower steady signal (between time t_1 and t_2) was recorded. The 1st shock velocity ($U_{s1,\text{LiF}}$) in the LiF-1 was obtained from the optical radiation signal. The DPS application allowed for direct measurement of the particle velocity of the foil. In fact, the latter almost remained the same as the particle velocity ($U_{p1,\text{LiF}}$) in the LiF-1 because the shock impedance of the aluminum foil approximately matched with that of the LiF. The 2nd shock particle velocity ($U_{p2} = U_{p1,\text{LiF}}$), the pressure ($P_2 = P_{1,\text{LiF}} = \rho_{0,\text{LiF}} U_{s1,\text{LiF}} U_{p1,\text{LiF}}$), and the density (ρ_2) of argon could be deduced by the continuity condition at the interface.

(III) The 4th shock particle velocity of argon was measured by the DPS technique, where the 2nd step signal of DPS expressed the aluminum foil movement ($U_{p2,\text{LiF}}$) again by the 2nd shock wave in the LiF-1. The detailed trajectories of the shock fronts are shown in Fig. 2(b). The 4th shock particle velocity ($U_{p4} = U_{p2,\text{LiF}}$) and the pressure ($P_4 = P_{2,\text{LiF}}$) was obtained by the LiF reshock state and continuity condition at interface (the detailed steps described in Ref. 4). With the shock wave propagated into the LiF-2 and the sapphire window, the observed radiance signal gradually became weaker due to the transparency loss of the interface (see time t_2 and t_3 in Fig. 2(a)). Moreover, the 3rd shock states could not be directly determined from the experimental signals, but could be obtained by analyzing the interactions among the waves.

In order to clarify the interaction procedure of the shock waves in detail, the position–time schematic diagram with the driveplate, the specimen, the LiF-1, and the LiF-2 are presented in Fig. 2(b), which shows the trajectories of the shock fronts and the interfaces under multishock compression. The several

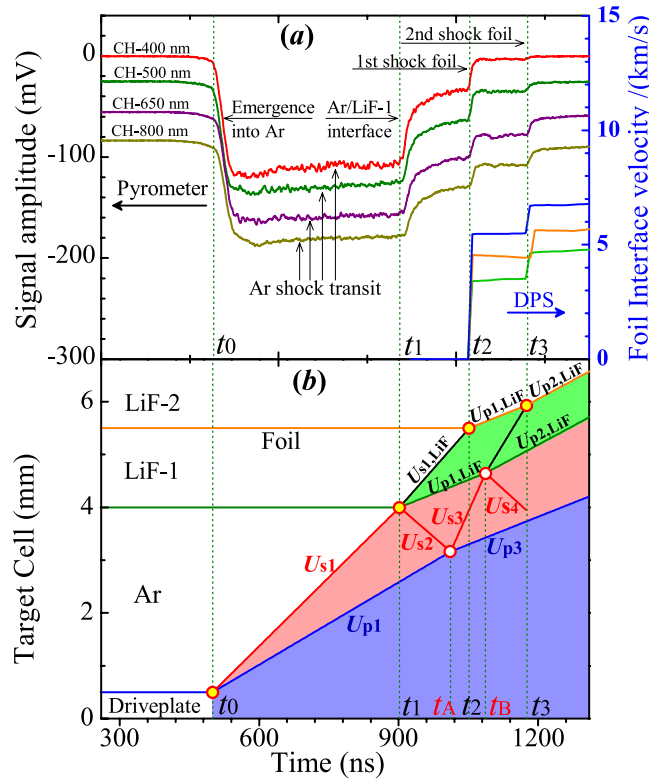


Figure 2. Typical experimental signals and corresponding characteristics for the shot of No. GAR-4. (a) self-emission spectral radiance by the pyrometer and interface particle velocity of the foil by DPS. The shock front arrival at the driveplate/Ar interface (t_0), the Ar/LiF-1 interface (t_1), the 1st shock front in LiF-1 arrival at Al foil (t_2), and 2nd shock front in LiF-1 arrival at Al foil (t_3). (b) Position-time characteristic diagram showing the trajectories of the shock fronts and interfaces. The corresponding time t_0 , t_1 , t_2 , and t_3 are the same as in (a). The time t_A and t_B could be deduced by the shock reverberation interaction and discussed in the Sec. III.

events of the shock with different interfaces interaction (see time t_0 , t_1 , t_2 , and t_3) are justly corresponding to the experimental signal jump of Fig. 2(a). However, the shock reverberation interactions at the driveplate/Ar interface (time t_A) and Ar/LiF-1 interface (time t_B) cannot be observed. The reverberation time is very important to acquire the 3rd shock state of argon. It can be indirectly deduced by the observed particle velocity, the shock velocity and time points to determine the integrated multishock compression states.

Multiple shock compression is an effective technique to acquire high-pressure state. For the transparent specimen, the states of argon can be analyzed combining the spectral radiance histories and interface particle velocity profile histories in our work. For the opaque or partially transparent argon under multishock compression, the states could be determined by means of the interface time and continuity condition. However, if the time when the shock meets the interface could not be determined rigorously, such as the shock reverberation time at the driveplate/Ar interface, the 3rd shock state determination will become difficult to acquire the whole states from 1st to 4th compression.

The 1st, 2nd, and 4th shock states determination has been illustrated in section II of this paper. Although the 4th shock pressure and particle velocity have been deduced by the DPS, the integrated 4th shock states including the shock wave velocity (U_{s4}) and the density (ρ_4) were not obtained. These status messages depend on the third-shock state, which was determined as follows. Firstly, according to the observed 2nd shock particle velocity and the pressure of argon, the 2nd shock wave velocity (U_{s2}) was acquired by the momentum conservation relation:

$$P_2 - P_1 = \rho_1 (U_{s2} - U_{p1}) (U_{p2} - U_{p1}) \quad (1)$$

Similarly, the 2nd shock velocity of LiF-1 ($U_{s2,LiF}$) was given by

$$P_{2,LiF} - P_{1,LiF} = \rho_{1,LiF} (U_{s2,LiF} - U_{p1,LiF}) (U_{p2,LiF} - U_{p1,LiF}) \quad (2)$$

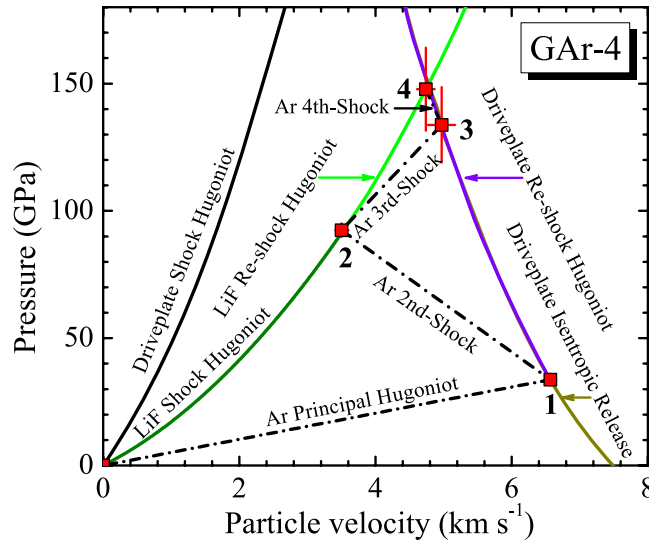


Figure 3. Impedance matching method used to obtain multishock pressure and particle velocity (shot of No. GAr-4). The solid red square symbols indicate the observed states of argon.

The shock reverberation interaction time at the driveplate/Ar interface (time t_A) and Ar/LiF-1 interface (time t_B) was indirectly obtained by the following method. Based on the shock and reshock wave interactions of argon in the Fig. 2(b), the compression process from time t_0 to time t_A (in Euler coordinate) was written as

$$U_{s1}(t_1 - t_0) + U_{s2}(t_A - t_1) = U_{p1}(t_A - t_0) \quad (3)$$

Meanwhile, the shock and reshock interaction processes of LiF-1 from time t_1 to time t_3 in Fig. 2(b) were written as

$$U_{s1,LiF}(t_2 - t_1) + U_{p1,LiF}(t_3 - t_2) = U_{p1,LiF}(t_B - t_1) + U_{s2,LiF}(t_3 - t_B) \quad (4)$$

According to Eqs. (3) and (4), the shock reverberation interaction time t_A and t_B was acquired. The whole interaction process occurring between the driveplate and LiF-1 anvil was clearly obtained. With the aid of the 2nd and 3rd shock displacement movement of argon in Fig. 2(b), the 3rd shock velocity (U_{s3}) was determined by

$$U_{s2}(t_A - t_1) + U_{s3}(t_B - t_A) = U_{p1,LiF}(t_B - t_1) \quad (5)$$

The 3rd shock states including the 3rd shock pressure (P_3), the density (ρ_3), and the particle velocity (U_{p3}) of argon were acquired by the impedance matching method in Fig. 3, and the 4th shock density (ρ_4) was given by

$$(U_{p4} - U_{p3})^2 = (P_4 - P_3)/(1/\rho_3 - 1/\rho_4) \quad (6)$$

The measured uncertainty for the 3rd shock velocity was determined as follow

$$\delta U_{s3} = \sqrt{\left(\frac{\partial U_{s3}}{\partial U_{s2}} \cdot \delta U_{s2}\right)^2 + \left(\frac{\partial U_{s3}}{\partial U_{p1,LiF}} \cdot \delta U_{p1,LiF}\right)^2 + \left(\frac{\partial U_{s3}}{\partial t_A} \cdot \delta t_A\right)^2 + \left(\frac{\partial U_{s3}}{\partial t_B} \cdot \delta t_B\right)^2} \quad (7)$$

where the uncertainties for the velocity and the time, such as δU_{s2} , $\delta U_{p1,LiF}$, δt_A , and δt_B were obtained from Eqs. (1)–(3). Also the 3rd shock pressure, the density, and the particle velocity with the uncertainties could be determined by impedance matching method.

The integrated multishock compression states (from 1st to 4th) are listed in Table 1, and the typical results by the impedance matching are shown in Fig. 3. The experimental pressure range of about 150 GPa and the density of about 5.3 g/cm³ are presented for warm dense argon, where the 4th shock state approaching to the final equilibrium state can be seen.

Shock temperature data can provide an important validation for the theoretical model. Using the absolute spectral radiance, $I(\lambda)$, of shock front, the single-shock temperature for argon can be extracted from the Planck radiation spectrum:

Shot No.	W (km/s)	Initial state		1st-shock					2nd-shock				3rd-shock				4th-shock		
		P_0 (MPa)	ρ_0 (g/cm ³)	U_{s1} (km/s)	U_{p1} (km/s)	P_1 (GPa)	ρ_1 (g/cm ³)	T_1 (kK)	$U_{s1,LiF}$ (km/s)	U_{p2} (km/s)	P_2 (GPa)	ρ_2 (g/cm ³)	U_{s3} (km/s)	U_{p3} (km/s)	P_3 (GPa)	ρ_3 (g/cm ³)	U_{p4} (km/s)	P_4 (GPa)	ρ_4 (g/cm ³)
GAr-1	4.53 ± 0.02	40.20 ± 0.01	0.584 ± 0.001	7.09 ± 0.07	4.94 ± 0.04	20.5 ± 0.2	1.93 ± 0.05	17.2 ± 1.6	8.43 ± 0.25	2.43 ± 0.06	54.1 ± 2.1	3.03 ± 0.19	8.54 ± 1.15	3.86 ± 0.08	80.4 ± 6.0	3.95 ± 0.35	3.54 ± 0.12	94.6 ± 11.5	4.07 ± 0.40
GAr-2	5.13 ± 0.03	40.50 ± 0.01	0.640 ± 0.001	7.76 ± 0.08	5.52 ± 0.04	27.5 ± 0.3	2.22 ± 0.07	18.8 ± 1.8	8.95 ± 0.27	2.81 ± 0.06	66.4 ± 2.5	3.83 ± 0.30	9.42 ± 1.85	4.25 ± 0.14	102.8 ± 11.6	4.90 ± 0.56	4.01 ± 0.08	114.2 ± 10.9	5.02 ± 0.64
GAr-3	5.63 ± 0.03	40.50 ± 0.01	0.638 ± 0.001	8.20 ± 0.05	6.06 ± 0.04	31.7 ± 0.3	2.45 ± 0.06	23.3 ± 2.5	9.60 ± 0.19	3.21 ± 0.09	81.4 ± 2.8	4.08 ± 0.30	9.92 ± 2.08	4.62 ± 0.16	120.2 ± 13.7	5.17 ± 0.60	4.40 ± 0.14	131.8 ± 16.4	5.29 ± 0.70
GAr-4	6.07 ± 0.03	40.05 ± 0.01	0.592 ± 0.001	8.66 ± 0.05	6.57 ± 0.05	33.7 ± 0.3	2.45 ± 0.07	23.4 ± 2.6	10.00 ± 0.14	3.50 ± 0.09	92.4 ± 2.7	4.04 ± 0.28	10.46 ± 2.22	4.97 ± 0.17	133.8 ± 14.8	5.12 ± 0.59	4.74 ± 0.13	147.8 ± 16.3	5.22 ± 0.66

Table 1. Multishock compression experimental data for dense gaseous argon. W is the flyer velocity. P , ρ , T , U_s , and U_p are the pressure, the density, the temperature, the shock and particle velocities in the argon, respectively. The subscripts 0, 1, 2, 3, and 4 represent the initial, single-, double-, third-, and fourth-shock states, respectively. $U_{s1,LiF}$ is the shock velocity in the LiF-1. The single-shock temperature is measured.

$$I(\lambda) = \varepsilon(\lambda) \frac{2\pi hc^2}{\lambda^5} \left(\exp\left(\frac{hc}{\lambda k_B T}\right) - 1 \right)^{-1} \quad (8)$$

where T is the radiation temperature, c , λ , h , and k_B represent the speed of light, the wavelength, the Planck constant, and the Boltzmann constant, respectively. $\varepsilon(\lambda)$ is the wavelength-dependent emissivity. In fact, the $\varepsilon(\lambda)$ depended strongly upon the wavelength, the radiation temperature, the shock front state, and the homogeneity. Since the current measuring range (400–800 nm) is far from the peak wavelength of the Planck distribution, the directly fitted values of the temperature by pyrometry will vary with the variation of the emissivity. Even small errors in the emissivity may greatly influence the fitted temperature values.

In current work, $\varepsilon(\lambda)$ was estimated by the reflectivity of shock front, $R(\lambda)$, with the relationship of $\varepsilon(\lambda) = 1 - R(\lambda)$. The $R(\lambda)$ was related to the complex refractive index of shock front, \hat{n}_s , which was calculated by the Drude model for warm dense matter. In the free-electron approximation the complex refractive index is written as²⁶,

$$\hat{n}_s^2 = 1 - \frac{\omega_p^2}{(2\pi c/\lambda)^2} (1 + i\lambda/2\pi c\tau_e)^{-1} \quad (9)$$

where $\omega_p = (4\pi n_e e^2/m_e)^{1/2}$ is the plasma frequency, and $\tau_e = R_0/v_f$ is the electron relaxation time. The parameters of n_e , m_e , and e denote the electron density, the electron mass, and the electron charge, respectively. R_0 is the electron mean-free path, which is limited to the interatomic distance. $v_f = \hbar(3\pi^2 n_e)^{1/3}/m_e$ is the Fermi velocity and \hbar is the Planck constant. n_e is necessary to obtain with the calculations. In virtue of Eq. (9), the refractive index \hat{n}_s can be obtained. The reflectivity $R(\lambda)$ is estimated from the Fresnel's formula, $R(\lambda) = |(\hat{n}_s - n_0)/(\hat{n}_s + n_0)|^2$, where n_0 is the refractive index in the initial precompressed argon. The emissivity $\varepsilon(\lambda)$ can be approximately estimated from the $R(\lambda)$, and the single-shock temperature is obtained from the nonlinear least squares fit. Figure 4 shows the estimated wavelength-dependent emissivity and the experimental radiance fits for shot of No. GAr-4. Table 1 presents the fitted single-shock temperature values in our work.

Discussion

For the diagnostics of multishock compression states, the target design is crucially important. It is necessary to avoid the influence of rarefaction and catch-up waves on the compressed samples. In our experiments, the wide-thick ratios of the targets were optimized by the calculation of the Lagrangian hydrodynamic equations based on the Riemann solver. Figure 5 shows the calculated trajectories of shock and rarefaction waves and the target interface movement in one-dimensional hydrodynamic simulation for the shot of No. GAr-4. It reveals that the catch-up rarefaction wave makes no influence on both the multishock reverberation diagnostics of dense argon plasma and the shock and reshock compression of LiF-1.

Four experiments were performed with the compressed states probed by a multichannel optical pyrometer and a velocity interferometer system. Table 1 shows the integrated multishock compression states of argon. The states span in the pressure-density ranges of 20–150 GPa and 1.9–5.3 g/cm³. The single-shock temperatures determined from the spectral radiance are also listed in Table 1. It is difficult to obtain multishock temperatures from the radiance due to the partial transparency loss of the interface. Hereby, the multishock temperatures are calculated using a model based on the self-consistent fluid

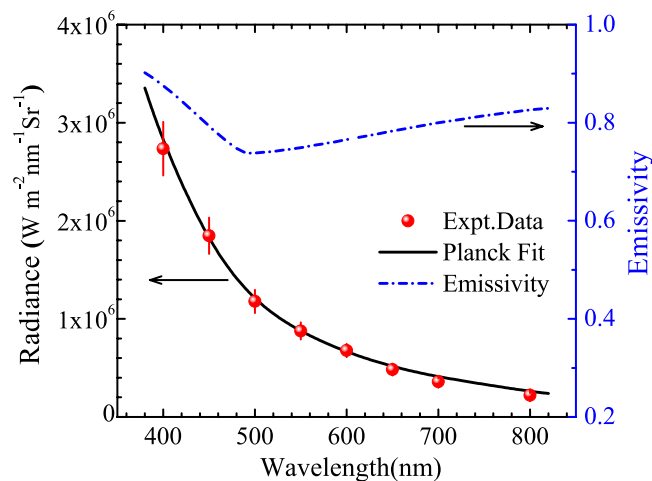


Figure 4. Experimental spectral radiance and the Planck radiation fitting ($T_1 = 23.4 \pm 2.6$ kK) for shot No. GAR-4. The wavelength-dependent emissivity is calculated and related to the reflectivity by the Drude model.

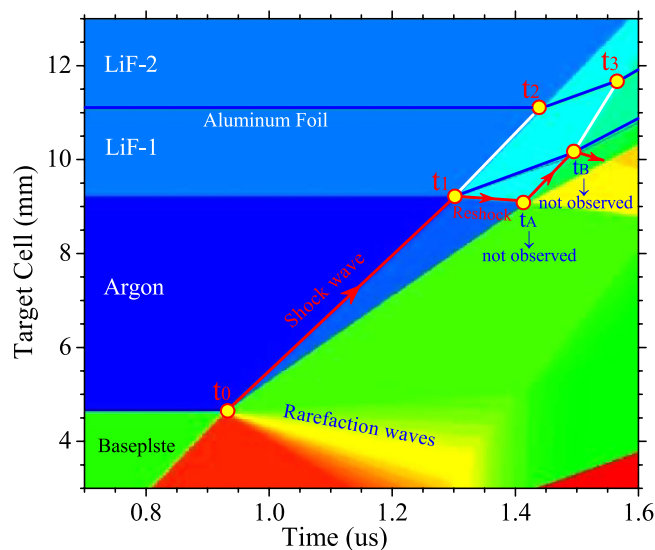


Figure 5. Position-time diagram by one-dimensional hydrodynamic simulation for the trajectories of the shock fronts and interfaces. t_0 , t_1 , t_2 , and t_3 can be observed by the pyrometer and the DPS. (Symbol meanings as same as Fig. 2).

variational theory (SFVT)^{17,27}. In chemical ionization equilibrium, the SFVT model introduced a correlative correction of the ionization energy by fulfilling self-consistency, and considering the interaction between the particles (*i.e.*, the atoms, ions, and electrons). This model could reproduce the experimental Hugoniot states of liquid argon²⁷, and predict the EOSs and ionization degree of fluid argon. Table 2 shows the calculated results, including the temperature, the ionization degree, the electron density, the coupling and the degeneracy parameters of dense argon plasma. These calculations could be compared with the experiments and characterize the physical properties under multishock compression.

In order to address the thermodynamic properties of multishock argon, the shock pressure versus the volume from 1st to 4th shock compression in this work are shown in Fig. 6, in comparison with previous results whose initial states are argon in the gas^{10,28}, liquid^{9,10}, and solid phase^{8,29}. It is observed that current experimental EOSs results extend the shock pressure to 150 GPa. The molar volume in the range of 7.5–21.0 cm³/mol (corresponding to the density of 1.9–5.3 g/cm³) was determined by virtue of the multishock reverberation technique. The shock temperatures in the range of 17.2–29.7 kK were also shown as an inset to Fig. 6, with single-shock data determined experimentally and other data given by the model. Fig. 6 also shows the calculated multishock curves approximately reflected from the

Shot No.	1st-shock					2nd-shock					3rd-shock					4th-shock				
	$T_{1,cal}$	α_1	$n_{e,1}$	Γ_1	Θ_1	$T_{2,cal}$	α_2	$n_{e,2}$	Γ_2	Θ_2	$T_{3,cal}$	α_3	$n_{e,3}$	Γ_3	Θ_3	$T_{4,cal}$	α_4	$n_{e,4}$	Γ_4	Θ_4
GAr-1	19.5	7%	0.2×10^{22}	2.1	2.4	22.4	25%	1.1×10^{22}	3.0	0.83	23.6	38%	2.3×10^{22}	3.4	0.62	23.9	47%	2.9×10^{22}	3.4	0.60
GAr-2	21.2	11%	0.4×10^{22}	2.5	1.5	23.2	29%	1.7×10^{22}	3.4	0.64	24.9	43%	3.2×10^{22}	3.6	0.54	25.3	50%	3.8×10^{22}	3.6	0.54
GAr-3	22.7	13%	0.5×10^{22}	2.6	1.1	25.2	34%	2.1×10^{22}	3.3	0.62	26.9	46%	3.6×10^{22}	3.5	0.54	27.4	51%	4.1×10^{22}	3.5	0.54
GAr-4	24.3	16%	0.6×10^{22}	2.6	1.1	27.8	37%	2.3×10^{22}	3.0	0.67	29.3	48%	3.7×10^{22}	3.2	0.56	29.7	51%	4.0×10^{22}	3.2	0.56

Table 2. The calculated dense argon plasma parameters under multi-shock compression. T , α , n_e , Γ , and Θ are the shock temperature, ionization degree, electron density, the coupling parameter, and the degeneracy for argon, respectively. The temperature in a unit is kilo-Kelvin. The electron density in a unit is cm^{-3} . The subscripts 1, 2, 3, and 4 meanings are as same as Table. 1.

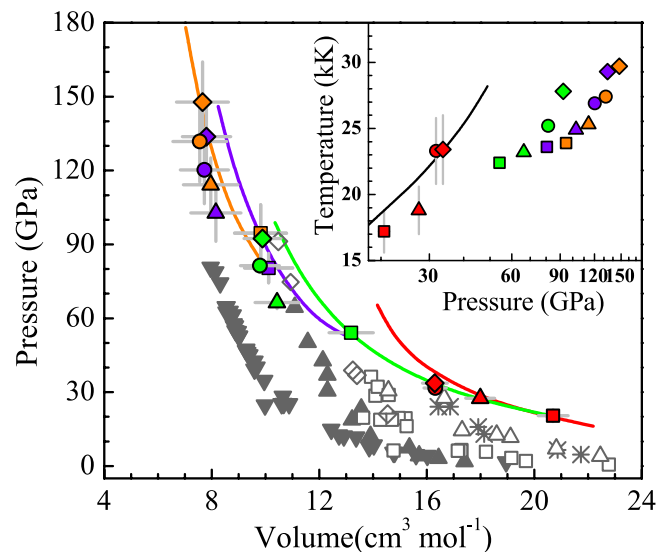


Figure 6. Comparison of argon shock data for different initial states and isotherm data for solid argon. The colored symbols represent the data of our work in the 1st (red), 2nd (green), 3rd (violet), and 4th (orange) shock compression. The solid curves were calculated from the corresponding lowest pressure point. For comparison, the dense argon results (open triangles²⁸ and stars¹⁰), the liquid argon (open diamonds⁹ and open squares¹⁰), the solid argon Hugoniot (solid triangles⁸) and the solid argon isotherm (inverted solid triangles²⁹) are also shown. Inset: The temperatures versus the pressure in our work are represented. The 1st shock data are measured and other data are calculated. The solid curve is the Hugoniot curve given by calculation.

corresponding lowest experiment points by the SFVT model. It is found that, the calculations are in good agreement with the experimental data within uncertainty of about 13%.

Until now single-shock compression of WDM has been investigated intensively^{8–12}. However, multishock compression, especially the change of compression ratios with the compression sequence has less been reported. Figure 7(a) shows the experimental results of argon with the multishock pressure versus the compression ratio ($\eta_i = \rho_i / \rho_0$, where $i = 1, 2, 3, 4$ is from 1st to 4th shock states, respectively). With the increase of the pressure, the compression ratio increases gradually from 3.3 to 8.8. It indicates that multishock reverberation technique could efficiently enhance the compression.

Figure 7(b) shows the comparison of experimental data of argon between the multishock pressure and the relative compression ratio ($\eta_i' = \rho_i / \rho_{i-1}$). An interesting phenomena is found in the relationship between the pressure and the relative compression ratio from the 1st to the 4th shocked states for the four groups of experiments. For the 1st shocked states, a higher pressure is associated with a higher relative compression ratio; for the 3rd and 4th compression states, a higher pressure is associated with a lower relative compression ratio. The turning point (corresponding to the maximum relative compression ratio $\eta_{2, \max}' = \rho_2 / \rho_1 \sim 1.70$) occurs at the 2nd shocked states, which shows a non-monotonous relationship between pressure and the relative compression ratio. This phenomenon is more clearly evidenced by our previous experimental results⁴ as is shown by the hollow symbols in Fig. 7(b). A similar phenomenon was also reported for the single and double shock of liquid deuterium¹³ as shown in the inset of Fig. 7. For double shock experiments of deuterium, a higher pressure is associated with a lower relative

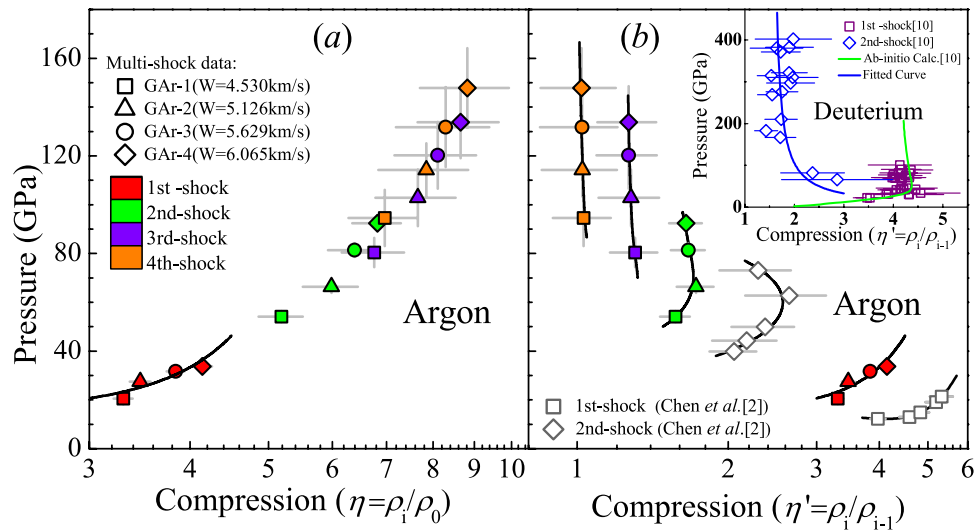


Figure 7. Comparison of multishock compression for gas argon in our present and previous work⁴. (a) the compression ratio ($\eta_i = \rho_i/\rho_0$, where $i = 1, 2, 3, 4$) and (b) the relative compression ratio ($\eta'_i = \rho_i/\rho_{i-1}$, where $i = 1, 2, 3, 4$) are corresponding with the 1st to 4th shock states, respectively. The present four shots data are described as the solid squares (GAr-1), the solid triangles (GAr-2), the solid circles (GAr-3), and the solid diamonds (GAr-4). Multishock experiments are also shown by the 1st (red), 2nd (green), 3rd (violet), and 4th shock (orange) results. The solid curves are fitted from experimental data at the corresponding states. Inset: Single-shock (open squares) and double-shock (open diamonds) compression of liquid deuterium by Z-accelerator¹³ is represented to illustrate the multishock compression.

compression ratio, while for single shock experiments, the relative compression ratio increases with pressure in the low pressure regime and decreases with pressure in the high pressure regime.

In general, the shock compression is controlled by two factors: the internal degree of freedom and the interaction of particles⁶. On the one hand, the total energy of shock wave goes up with the increase of the flyer velocity. It will lead to the enhanced excitation of internal degrees of freedom and the increased ionization in absorbing the thermal energy in the system, which increase the compression. On the other hand, the increase in flyer velocity leads to the increase in the ionization degree and the number density of particles in the system, which could enhance the repulsive interactions between particles and reduce the compression. Therefore, the maximum relative dynamic compression begins to appear at the dominant of atomic excitation in these two effects. Subsequently, with further increase in multishock pressure, a rise number of particles due to the ionization result in the increase in particles repulsive interactions and the decrease in relative compression ratio.

In order to illustrate thermophysical properties of argon plasma under multishock compression, especially the thermal-induced effect in warm dense regime, the coupling parameter (Γ) and the degeneracy parameter (Θ) of argon by SFVT calculations are plotted in the temperature-density plane in Fig. 8, as well as the current experimental results. Multishock compressed dense argon plasma with the ionization degree, the coupling parameter, and the degeneracy is presented in Table 2. For multishock states under different flyer impact velocities, the maximum Γ and the minimum Θ are not appeared at highest pressure regime. As we known, the Γ is the ratio of the interaction potential energy to kinetic energy, which reflects on the evolution of potential and kinetic energies in multishock process. In Fig. 8 it can be seen that the Θ values are mostly around 1, and coupled parameter in the range of $2.0 < \Gamma < 4.0$. Therefore, the present multishock compression states are mostly degenerate, strongly coupled, and nonideal, which have entered into warm dense regime. These multishock data are very useful for creating new theoretical models and checking existing ones of warm dense matter.

In summary, warm dense argon was produced via the multishock reverberation technique, and the integrated diagnostics from single-shock to fourth-shock states at the pressure of 150 GPa and the density of 5.3 g/cm³ were performed. The current experimental results indicated that the compression could effectively enhanced from 3.3- to 8.8-fold by multiple compression. The limited relative compression ratio $\rho_2/\rho_1 \sim 1.70$ was observed at double-shock states, subsequently the 3rd and 4th compression slightly decreased with increasing pressure. The evolution of the compression reflects on the interaction effects between particles and on the changes of the excitation of internal degrees of freedom, the ionization, the potential and kinetic energies in multishock-compressed dense argon process. The thermodynamic physical properties of warm dense argon were characterized with the EOSs, compression, coupled, and degenerate parameters. The current diagnostic technique and the calculated model for warm dense argon can be applied to other dense gas, such as rare gases, H₂, O₂, and N₂.

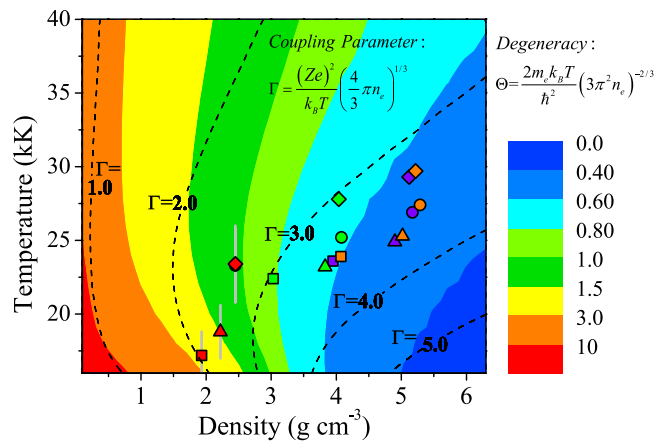


Figure 8. The contours of degenerate (Θ) and coupling parameters (Γ) of dense argon in the P - ρ plane. The current multiple shock compression observed results up to warm dense matter regime are also presented. (Symbol meanings are as same as Fig. 7).

Methods

The initial precompressed argon was confined in a sandwich assembly including the driveplate, the specimen cell, and the anvils, as schematically shown in Fig. 1. In order to achieve high homogeneity and avoid the influence of rarefaction and catch-up waves, the specimen target design was optimized with the flyer, the driveplate, the sample chamber, and the anvils by the hydrodynamic simulation. By means of the accelerating flyer technique in a two-stage light gas gun, warm dense argon was produced by shock wave. The shock was generated at the interface of the flyer (~3.20 mm thick, tantalum) and the driveplate (~5.00 mm thick, stainless steel 304), and then the shock passed through argon specimen (~4.00 mm thick). The rear of the assembly consisted of two LiF “anvils” and a median aluminum foil. The anvil interface was glued with transparent epoxy Plexiglas. The anvil close to specimen (labeled in LiF-1, ~1.50 mm thick) was used to protect the foil from thermal ablation under shock compression. The other anvil (labeled in LiF-2, ~4.00 mm thick) was plated by the aluminum foil with the front surface outside (~4 mm in diameter central area), which was served as a laser reflective coating in the interface velocity interferometry by the DPS. The sapphire window was employed to prevent the LiF anvils from pre-compressed fracture. Considering the interaction of the waves at the interface, the shock wave in the argon specimen would propagate and reverberate between the driveplate and the LiF-1 with higher shock impedance.

References

- Glenzer, S. H. *et al.* Observations of Plasmons in Warm Dense Matter. *Phys. Rev. Lett.* **98**, 065002 (2007).
- Koenig, M. *et al.* Progress in the study of warm dense matter. *Plasma Phys. Control. Fusion* **47**, B441 (2005).
- Li, D. F. *et al.* Quantum molecular dynamics study of expanded beryllium: Evolution from warm dense matter to atomic fluid. *Sci. Rep.* **4**, 5898 (2014).
- Chen, Q. F. *et al.* Thermophysical properties of multi-shock compressed dense argon. *J. Chem. Phys.* **140**, 074202 (2014).
- Vorberger, J., Donko, Z., Tkachenko, I. M. & Gericke, D. O. Dynamic Ion Structure Factor of Warm Dense Matter. *Phys. Rev. Lett.* **109**, 225001 (2012).
- Driver, K. P. & Militzer, B. First-principles simulations and shock Hugoniot calculations of warm dense neon. *Phys. Rev. B* **91**, 045103 (2015).
- Loubeyre, P. *et al.* Extended data set for the equation of state of warm dense hydrogen isotopes. *Phys. Rev. B* **86**, 144115 (2012).
- Dick, R. D., Warnes, R. H. & JR. & J. Skalyo. Shock Compression of Solid Argon. *J. Chem. Phys.* **53**, 1648 (1970).
- Nellis, W. J. & Mitchell, A. C. Shock compression of liquid argon, nitrogen, and oxygen to 90 GPa (900 kbar). *J. Chem. Phys.* **73**, 6137 (1980).
- Thiel, M. van & Alder, B. J. Shock Compression of Argon. *J. Chem. Phys.* **44**, 1056 (1966).
- Ross, M. The repulsive forces in dense argon. *J. Chem. Phys.* **73**, 4445 (1980).
- Nellis, W. J. *et al.* Shock Compression of Liquid Helium to 56 GPa (560 kbar). *Phys. Rev. Lett.* **53**, 1248 (1984).
- Knudson, M. D. *et al.* Principal Hugoniot, reverberating wave, and mechanical reshock measurements of liquid deuterium to 400 GPa using plate impact techniques. *Phys. Rev. B* **69**, 144209 (2004).
- Zheng, J., Chen, Q. F., Gu, Y. J. & Chen, Z. Y. Hugoniot measurements of double-shocked precompressed dense xenon plasmas. *Phys. Rev. E* **86**, 066406 (2012).
- Militzer, B. Path integral Monte Carlo and density functional molecular dynamics simulations of hot, dense helium. *Phys. Rev. B* **79**, 155105 (2009).
- Militzer, B. & Ceperley, D. M. Path integral Monte Carlo calculation of the deuterium Hugoniot. *Phys. Rev. Lett.* **85**, 1890 (2000).
- Chen, Q. F., Cai, L. C., Gu, Y. J. & Gu, Y. Ionization and equation of state of dense xenon at high pressures and high temperatures. *Phys. Rev. E* **79**, 016409 (2009).
- Gu, Y. J. *et al.* Multishock comparison of dense gaseous H₂+He mixtures up to 30 GPa. *J. Chem. Phys.* **130**, 184506 (2009).
- Gu, Y. J. *et al.* The equation of state, shock-induced molecule dissociation, and transparency loss for multi-compressed dense gaseous H₂+D₂ mixtures. *J. Appl. Phys.* **111**, 013513 (2012).
- Ternovoi, V. Ya. *et al.* Thermodynamic properties and electrical conductivity of hydrogen under multiple shock compression to 150 GPa. *Physica B* **265**, 6 (1999).

21. Ternovoi, V. Ya. *et al.* Thermophysical Properties of Helium under Multiple Shock Compression. *AIP Conf. Proc.* **620**, 107 (2002).
22. Ternovoi, V. Ya. *et al.* Experimental Determination of the Conditions for the Transition of Jupiter's Atmosphere to the Conducting State. *JETP Lett.* **79**, 6 (2004).
23. Zheng, J., Gu, Y. J., Chen, Z. Y. & Chen, Q. F. Measurements of the equations of state and spectrum of nonideal xenon plasma under shock Compression. *Phys. Rev. E* **82**, 026401 (2010).
24. Weng, J. D. *et al.* Optical-fiber interferometer for velocity measurements with picoseconds Resolution, *Appl. Phys. Lett.* **89**, 111101 (2006).
25. Duvall G. E. & Graham R. A. Phase transitions under shock-wave loading. *Rev. Mod. Phys.* **49**, 523 (1977).
26. Collins, G. W. *et al.* Temperature Measurements of Shock Compressed Liquid Deuterium up to 230 Gpa. *Phys. Rev. Lett.* **87**, 165504 (2001).
27. Chen, Q. F. *et al.* Equation of state of partially ionized argon plasma. *Phys. Plasmas* **18**, 112704 (2011).
28. Thiel, M. van. Compendium of shock wave data, LLNL Report, *UCRL-50108* (1977), p. 9.
29. Ross, M., Mao, H. K., Bell, P. M. & Xu, J. A. The equation of state of dense argon: A comparison of shock and static studies. *J. Chem. Phys.* **85**, 1028 (1986).

Acknowledgements

We thank our colleagues for the gas gun operation, the experimental diagnosis, and the devices. Our work was supported by the National Natural Science Foundation of China under Grant No. 11074226, by the Science and Technology Development Foundation of China Academy of Engineering Physics under Grant No. 2013A0101001, 2014B0102003, 2015B0102001, and 201501032, and the foundation of Laboratory of Shock Wave and Detonation Physics, CAEP under Grant No. 9140C670103130C67235, 9140C670104120C6747, and 9140C670103150C67001.

Author Contributions

J.Z. wrote the paper and did the experiments. Q.C., Y.G. and Z.L. analyzed the results. Z.S. did the calculations.

Additional Information

Competing financial interests: The authors declare no competing financial interests.

How to cite this article: Zheng, J. *et al.* Multishock Compression Properties of Warm Dense Argon. *Sci. Rep.* **5**, 16041; doi: 10.1038/srep16041 (2015).



This work is licensed under a Creative Commons Attribution 4.0 International License. The images or other third party material in this article are included in the article's Creative Commons license, unless indicated otherwise in the credit line; if the material is not included under the Creative Commons license, users will need to obtain permission from the license holder to reproduce the material. To view a copy of this license, visit <http://creativecommons.org/licenses/by/4.0/>